Astrocyte-Derived Extracellular Vesicles Alleviate Optic Nerve Injury Through Remodeling of Retinal Microenvironmental Homeostasis

Lili Chen,[1,2] Zhonghao Yu,[1,2] Senmiao Zhu,[1,2] Shihan Song,[1,2] Guanwen He,[1,2] Zai-Long Chi,[1,2] and Wencan Wu[1–3]

[1]State Key Laboratory of Ophthalmology, Optometry and Visual Science, Eye Hospital, Wenzhou Medical University, Wenzhou, China
[2]National Clinical Research Center for Ocular Diseases, Eye Hospital, Wenzhou Medical University, Wenzhou, China
[3]Oujiang Laboratory (Zhejiang Lab for Regenerative Medicine, Vision and Brain Health), Wenzhou, Zhejiang, China

Correspondence: Wencan Wu, National Clinical Research Center for Ocular Diseases, Eye Hospital, Wenzhou Medical University, 270 Xueyuan West Rd., Wenzhou, Zhejiang 325027, China; wuwencan@wmu.edu.cn.
Zai-Long Chi, State Key Laboratory of Ophthalmology, Optometry and Visual Science, Eye Hospital, Wenzhou Medical University, 270 Xueyuan West Rd., Wenzhou, Zhejiang 325027, China; zailong.chi@eye.ac.cn.

LC and ZY contributed equally to this work.

Received: November 8, 2024
Accepted: March 14, 2025
Published: April 7, 2025

Citation: Chen L, Yu Z, Zhu S, et al. Astrocyte-derived extracellular vesicles alleviate optic nerve injury through remodeling of retinal microenvironmental homeostasis. *Invest Ophthalmol Vis Sci.* 2025;66(4):16. https://doi.org/10.1167/iovs.66.4.16

Purpose. Traumatic optic neuropathy (TON) leads to the loss of retinal ganglion cells (RGCs) and results in permanent visual impairment. Protecting and regenerating RGCs is crucial for the treatment of TON. Studies have demonstrated that astrocyte-derived extracellular vesicles (ADEVs) exhibit neuroprotective effects in models of central nervous system (CNS) injury. This study aimed to investigate whether ADEVs have a similar neuroprotective effect on RGCs in an optic nerve crush (ONC) rat model.

Methods. ADEVs were collected from primary rat astrocytes, and an ONC model was established to evaluate the effects of ADEVs on retinal structure and visual function using optical coherence tomography (OCT), hematoxylin and eosin (H&E) staining, and flash visual evoked potential (f-VEP) analysis. Immunofluorescence was used to examine RGCs and investigate reactive gliotic changes. Additionally, miRNA sequencing of ADEVs and retinal mRNA sequencing were performed to identify the potential mechanisms involved.

Results. ADEVs protected RGCs from progressive loss and improved visual function. ADEVs also significantly increased the expression of glial fibrillary acidic protein (GFAP) and modulated microglial activation. The miRNAs associated with ADEVs were targeted by neuroprotective signals, such as MAPK, PI3K-AKT, and TNF-α, and through the targeting network generated via retinal mRNA sequencing, we found that potential functional genes, such as THBS1, PAK3, and Gstm1, likely participate in microenvironmental regulation.

Conclusions. We discovered that ADEVs play a neuroprotective role in optic nerve injury. Our findings provide a new cell-free therapeutic strategy for optic neuropathy.

Keywords: optic nerve injury, traumatic optic neuropathy (TON), astrocytes, extracellular vesicles (EVs), retinal ganglion cells (RGCs), degeneration, microglia, microRNA (miRNA), neuroprotection

Traumatic optic neuropathy (TON), caused by orbital, ocular, and head and face trauma, leads to irreversible blindness by inducing retinal ganglion cell (RGC) and axonal degeneration.[1,2] As an extension of the central nervous system (CNS), the optic nerve is formed by the nerve fiber layer extending from the RGCs, transmitting visual information from the retina to the brain.[3] Therefore, neuroprotective strategies focused on the vulnerable RGCs are highly desirable.

Retinal glial cells, including microglia, astrocytes, and Müller cells, play critical roles in modulating the pathological process of TON,[4] exerting both neuroprotective and neurotoxic effects on RGCs. Following optic nerve injury, astrocytes undergo reactive changes, termed astrogliosis, which can be classified into two phenotypes: the neurotoxic A1 phenotype and the neuroprotective A2 phenotype.[5,6] The balance between these phenotypes is essential, as early astrogliosis can provide neurotrophic support, whereas prolonged activation leads to detrimental effects on RGCs. Similarly, microglia, which migrate to the injury site, contribute to tissue repair but can exacerbate neuronal damage as sustained microglial activation can result in excessive production of proinflammatory cytokines and reactive oxygen species (ROS), exacerbating neuronal damage.[4,7] Interestingly, astrogliosis can recruit microglia to injury sites and, at later stages, exert anti-inflammatory effects by modulating microglial activation.[8] In addition, reactive Müller cells express neurotrophic factors in addition to brain-derived neurotrophic factor (BDNF), nerve growth factor (NGF), and glial cell line derived neurotrophic factor (GDNF), promoting RGC survival. Nevertheless, excessive proliferation of reactive Müller cells dramatically induces apoptosis and inflammation, causing neurodegeneration in retinal injury.[9,10]

Astrocytes, accounting for 20% to 50% of CNS cells, migrate into the retina along the developing optic nerve and are located primarily in the nerve fiber and ganglion cell layers. They are essential for maintaining the blood–retina barrier, releasing neurotrophic factors, and regulating synaptic plasticity to support RGC function.[8,11] Recent studies have shown that astrocyte transplantation can promote neuronal regeneration in CNS injuries.[12–14] However, challenges such as low survival rates and immune rejection limit the effectiveness of astrocyte-based therapies, thus we need to explore more appropriate strategies to minimize undesirable characteristics.

Astrocytes can influence neuronal survival in response to inflammation or oxidative stress through the release of extracellular vesicles (EVs).[15,16] EVs are nanosized, membrane-bound vesicles containing proteins, lipids, and nucleic acids that can be delivered to recipient cells. Their ability of EVs to cross the blood–brain barrier with low immunogenicity makes them promising therapeutic agents for CNS diseases.[17–19] Notably, EVs are able to elicit protective effects on RGCs,[20–25] suggesting their benefits on TON therapy. Therefore, astrocyte-derived extracellular vesicles (ADEVs) may offer a cell-free therapeutic approach, circumventing the limitations associated with direct astrocyte transplantation.

Both in vivo and in vitro investigations have highlighted the potential of ADEVs in promoting neuronal survival following CNS injuries. For example, Chun et al. reported that ADEVs enhanced the survival and electrophysiological function of cultured neurons by inhibiting apoptosis.[26] In animal models of traumatic brain injury, ADEVs have been shown to restore neuronal mitochondrial function, reduce neuronal atrophy, and mitigate oxidative stress.[27,28] Additionally, ADEVs have been shown to exert therapeutic effects in conditions such as ischemic stroke and spinal cord injury due to their immunomodulatory and neuroprotective properties.[16,29]

However, it remains unclear whether ADEVs can protect RGCs in TON. This study aimed to evaluate the effects of ADEVs on RGC survival using an optic nerve injury model and to explore the underlying molecular mechanisms involved.

Methods

Animals

Adult male Sprague–Dawley (SD) rats aged 8 weeks (weighing 180–200 g) and neonatal rats were purchased from Vital River Experimental Animal Technology (Beijing, China). All procedures conformed to the ARVO Statement for the Use of Animals in Ophthalmic and Vision Research and were approved by the Institutional Animal Care and Use Committee of Wenzhou Medical University (approval No. wydw2022-0078). The sham group is defined as rats that underwent optic nerve exposure without the crush operation, whereas the phosphate-buffered saline (PBS) or ADEV group consisted of rats that received unilateral optic nerve crush (ONC) surgery and were immediately intravitreally injected with either PBS or ADEVs.

Isolation and Cultivation of Primary Rat Astrocytes

Primary cortical astrocytes were obtained from neonatal rats as previously described.[30,31] Briefly, cortical tissues were digested with 0.25% trypsin-EDTA for 15 minutes at 37°C, and the samples were shaken gently every 5 minutes for adequate digestion. The cells were cultured in DMEM/F-12 (Gibco, USA) supplemented with 10% FBS (Gibco, USA) and 1% penicillin–streptomycin (Gibco, USA). On days 10 to 12, the flasks were shaken at 200 rpm for 1 hour to remove microglia and at 250 rpm for 24 hours to remove oligodendrocytes. Astrocytes were inoculated in poly-L-lysine-coated flasks in Astrocyte Medium-animals (AM-a, Sciencell, USA) supplemented with Astrocyte Growth Supplement, 2% FBS, and 1% penicillin–streptomycin. Cells from passages 1 to 3 were used. The human skin fibroblasts (FH0189, FuHeng, Shanghai, China) used as control cells were cultured in DMEM/F-12 (Gibco, USA) supplemented with 15% FBS and 1% penicillin–streptomycin at 37°C under 5% CO_2, and the cells from passages 2 to 5 were used.

EV Isolation

The methods used for research on EVs in this study adhered to the MISEV2023 guidelines.[32] EVs from astrocytes and fibroblasts were isolated by ultracentrifugation as previously described.[23] Briefly, astrocytes and fibroblasts were seeded at densities of 1.2×10^6 and 3×10^6 cells/mL, respectively. The conditioned medium was replaced with EV-depleted medium containing exosome-depleted FBS (System Biosciences, Palo Alto, CA, USA), which was added to the basal medium when cultured cells reached 70% to 80% confluence. After 72 hours of cultivation, the conditioned medium was collected and subjected to sequential differential centrifugation: 300*g* for 10 minutes to remove the floating cells, 2000*g* for 10 minutes to remove cell debris, and 10,000*g* for 30 minutes to remove microvesicles and apoptotic bodies. The pellet was discarded, and the supernatant was collected at each step. The collected supernatant was subsequently ultracentrifuged at 100,000*g* for 70 minutes at 4°C (SW32Ti rotor; Beckman Coulter, CA, USA) to isolate the EVs. The pellet was subsequently resuspended in PBS (pH 7.2) and ultracentrifuged again at 100,000*g* for 70 minutes at 4°C (SW41Ti rotor; Beckman Coulter, USA). Finally, the ADEVs and fibroblast-derived EVs were resuspended in 100 µL of PBS.

Nanoparticle Tracking Analysis

The concentrations and size distributions of ADEVs were characterized by a ZetaView Particle Metrix (PMX 110, Meerbusch, Germany) with a sensitivity setting of 70. The samples were prediluted 1:1000 in PBS, and particle movement in a 60-second video was analyzed using Nanoparticle Tracking Analysis (NTA) software (Zeta View 8.02.28).

Transmission Electron Microscopy

The collected ADEVs (10 µL) were deposited onto Lacey Formvar/carbon-coated copper grids and incubated at room temperature for 10 minutes. After being washed with sterile distilled water and dried for 2 minutes, the grids were observed and imaged via transmission electron microscopy (TEM; HITACHI, H-7650, Tokyo, Japan). Images were captured in 3 fields, and 2 photographs were captured for each of the fields at scales of 200 nm and 500 nm.

Table 1. Primary and Secondary Antibodies

Antibody	Description	Catalog Number	Dilution	Company
TSG101	Mouse monoclonal	PTM-5108	1:1000	PTM BIO, Hangzhou, China
Alix	Rabbit monoclonal	PTM-6407	1:1000	PTM BIO, Hangzhou, China
CD81	Rabbit monoclonal	PTM-6220	1:1000	PTM BIO, Hangzhou, China
Calnexin	Rabbit monoclonal	10427-2-AP	1:1000	Proteintech, Chicago, IL, USA
GFAP	Rabbit monoclonal	bs-0199R	1:500	Bioss, Beijing, China
Vimentin	Mouse monoclonal	sc-6260	1:500	Santa Cruz, Dallas, Texas, USA
RBPMS	Rabbit monoclonal	15187-1-AP	1:500	Proteintech, Chicago, IL, USA
Iba-1	Rabbit monoclonal	019-19741	1:500	Wako, Osaka, Japan
Goat anti-mouse Alexa Fluor 594		bs-0296G	1:500	Bioss, Beijing, China
Goat anti-rabbit Alexa Fluor 488		bs-0295G	1:500	Bioss, Beijing, China
HRP linked goat anti-mouse IgG (H+L)		10216	1:1000	Beyotime, Shanghai, China
Anti-rabbit HRP linked antibody		7074S	1:1000	Cell Signal Technology, Danvers, MA, USA

CD, cluster of differentiation; GFAP, glial fibrillary acidic protein; RBPMS, RNA binding protein with multiple splicing.

Western Blot Analysis

Total EV protein was extracted with RIPA buffer, and the protein concentration was measured with a Bicinchoninic Acid Protein Assay Kit (Thermo Scientific, Waltham, MA, USA). Equal amounts (4.5 µg) of astrocyte lysates and ADEV proteins were added to the same 10% sodium dodecyl sulfate–polyacrylamide (SDS–PAGE) gel to assess the enrichment/depletion of EVs and then transferred from the gel to PVDF membranes. The membranes were blocked with 5% nonfat dry milk buffer in PBS-Triton X-100 (PBST) for 2 hours and incubated with primary antibodies against TSG101, Alix, CD81, and Calnexin overnight at 4°C. Afterward, the membranes were incubated with HRP-conjugated secondary antibodies for 1 hour at room temperature and exposed using an Invitrogen iBright 1500 (iBright FL1500; Thermo Fisher Scientific). Table 1 contains the specific information for the antibodies mentioned in this article.

Optic Nerve Crush and Intravitreal Injection of EVs

The animals were anesthetized with 5% isoflurane (RWD Life Science, Guangdong, China; 0.8 Liters per minute O_2), which was maintained at 1% throughout the procedure. The optic nerve was sufficiently exposed through conjunctival fornix incision under a microscope (Leica, Wetzlar, Germany), and forceps (WA3010; Jinzhong, Shanghai, China) were used to crush the optic nerve at 2 mm posterior to the eyeball for 10 seconds. Immediately after surgery, 4 µL of PBS loaded with ADEVs or fibroblast-EVs at 1×10^9 particles was intravitreally injected slowly using a Hamilton syringe needle (33G; (Hamilton, NV, USA). The needle was inserted at the limbus and retracted after a 1-minute delay to minimize backflow.

Optical Coherence Tomography and Measurement of Ganglion Cell Complex Thickness

The rats were anesthetized with 150 mg/kg Avertin (T48402; Sigma–Aldrich, St. Louis, MO, USA). Tropicamide eye drops were applied to the eyes to dilate the pupils for 10 minutes, after which the rats were subjected to surface anesthesia with proparacaine hydrochloride eye drops. Optical coherence tomography (OCT) was subsequently performed at 0 (pre-ONC), 7, and 14 days postinjury via a Phenix Micron IV microscope (United States) or Heidelberg SPECTRALIS OCT (Germany). Retinal images were captured around the optic nerve head with a circular scan pattern. The scan size was set to 1800 µm around the optic disc to capture different retinal layers. Imaging and analysis were performed using the Micron IV Imaging Software or Heidelberg Eye Explorer. Levofloxacin eye cream was administered to moisten the cornea throughout the entire procedure. Ganglion cell complex (GCC) thickness was measured via the built in software.

Hematoxylin and Eosin Staining

The anesthetized rats were perfused transcardially with PBS and 4% paraformaldehyde (PFA). Eyeballs were fixed in ferrous ammonium sulfate (FAS) solution for 24 hours at room temperature. Paraffin-embedded eyeballs were cut into 3 µm slices, and those positioned in the optic nerve head were used for further staining. After dewaxing, the tissue slices were incubated with hematoxylin and eosin (H&E; C0105S, Beyotime Biotechnology). Images were obtained under a microscope with a 40 × objective, and the GCC thickness around the optic nerve head was measured via ImageJ software.

Immunofluorescence Staining

Rat eyeballs were dissected and fixed in PFA for 40 minutes at room temperature. The samples were embedded in optimal cutting temperature compound (Cat# 4583; Sakura, Oakland, CA, USA) and sectioned at 15 µm thickness using a cryostat (Leica CM 1950). Eye sections with visible optic nerve heads were selected to ensure consistency across samples. Then, the samples were treated with 0.5% PBST containing 10% goat serum at room temperature for 2 hours. Primary antibodies (rabbit anti-RBPMS, Iba1, and GFAP) were incubated with the samples overnight at 4°C. After washing, the sections were incubated with the secondary antibody (goat anti-rabbit Alexa Fluor 488) at room temperature for 1.5 hours in the dark. The slides were mounted with antifade mounting medium containing DAPI (Beyotime, Shanghai, China) and analyzed using a confocal microscope (Zeiss Cell Observer SD, Germany). The IBa 1+/RBPMS+ cell numbers were counted manually via ImageJ software. The GFAP fluorescence positive area quantification was performed using ImageJ software. Initially, outliers were removed using the "Remove Outliers" tool to eliminate interference from impurities. The "Thresh-

Investigative Ophthalmology & Visual Science

old" tool was then applied with default settings to delineate the GFAP fluorescence positive area. Finally, the percentage of the delineated positive area relative to the total image area was calculated and used as a quantitative value for statistical analysis. Antibody details are provided in Table 1.

Immunocytochemistry

Astrocytes were fixed with 4% PFA at room temperature for 15 minutes. After washing with PBS, the cells were incubated with PBS supplemented with 0.5% PBST for 2 hours at room temperature and then incubated overnight at 4°C with rabbit anti-GFAP and mouse anti-vimentin antibodies. Secondary antibodies were used to detect GFAP and vimentin. The nuclei were labeled with DAPI for 10 minutes at room temperature. Images were captured with a 20 × objective using a DM4B microscope (Leica, Wetzlar, Germany).

Flash Visual Evoked Potential Recording

Flash visual evoked potentials (f-VEPs) were recorded using an electrophysiological diagnostic apparatus (GT-2008V-III, GOTEC, Chongqing, China). The rats were allowed to adapt to the dark for 15 minutes and anesthetized with 5% isoflurane (0.8 L/min O_2), which was maintained at 3% during the procedure. Silver electrodes were implanted under the skin between the ears (recording electrode), into the cheek (reference electrode), and into the tail (ground electrode). White flash stimuli were delivered at 1.3 hertz (Hz) for a duration of 250 ms. The final waveform for each rat was obtained by averaging the responses from 64 tests. The N1-P1 amplitude was automatically measured, and the average of two stable waveforms was calculated for each rat. The contralateral eye was covered during recording.

Survival Count of RGCs

After immunofluorescence with the RBPMS, 4-leaf clover-shaped retinas were imaged with a 20 × objective using a Cell Observer SD confocal microscope. A total of 12 locations were selected, including 4 each in the central area (1 visual field), pericentral area (7 visual fields), and peripheral area (14 visual fields) from the optic nerve head (the side length of a visual field under a 20 × objective was 341.33 µm). Finally, the number of RGCs in three areas was calculated as the average for four locations via ImageJ software.

EV Tracking

ADEVs were fluorescently labeled with a PKH67 Cell Linker Kit (Sigma, St. Louis, MO, USA) following the manufacturer's instructions. The EV pellet was resuspended in 500 µL of dilution C, and 2 µL of PKH67 was added to another 500 µL of dilution C. The 2 solutions were mixed gently and incubated at room temperature for 5 minutes. Then, an equal volume (1 mL) of 0.5% bovine serum albumin was added to allow the removal of unincorporated dye contamination from the EV labeling reactions. Finally, PKH67-labeled ADEVs were resuspended in 100 µL of PBS following ultracentrifugation at 100,000*g* and 4°C for 70 minutes. The intravitreally injected labeled EVs were detected at 24 hours after injury.

miRNA Sequencing

ADEVs obtained from primary astrocyte cultures were sent to Beijing ECHO Biotech Company for processing and sequencing. Total RNA was extracted following the manufacturer's protocol, and the RNA concentration and purity were assessed using the Agilent Bioanalyzer 2100 system. For small RNA libraries, 1 to 500 ng of RNA was used as input material with the QIAseq miRNA Library Kit and index codes for sample identification. Library quality was evaluated using the Agilent Bioanalyzer 2100 and qPCR. Clustering was performed on an acBot Cluster Generation System using the TruSeq PE Cluster Kit v3-cBot-HS. Sequencing was conducted on an Illumina HiSeq platform, generating paired-end reads.

mRNA Sequencing

At 7 days post injury (dpi), fresh retinal samples were collected from the injured eyes of the ADEV-treated and PBS-treated groups and immediately frozen in liquid nitrogen. RNA extraction and sequencing were performed by a biotechnology company (Shanghai Biochip Co., Ltd., China). Total RNA from each sample was extracted using miRNeasy Micro Kit (QIAGEN, Germany) according to the manufacturer's instructions. The homogenate was then subjected to phase separation using chloroform to isolate RNA. After extraction, the RNA was purified and concentrated using RNeasy MinElute spin column, followed by elution in RNase-free water. To assess RNA quality, the RNA concentration and purity were measured using a Qubit. A ratio of approximately 2.0 for 260/280 nm is considered indicative of high-quality RNA. Additionally, RNA integrity was further assessed by running an aliquot of the RNA on a 4200 TapeStation to obtain the RNA integrity number (RIN). Only samples with RIN values above 7 were used for downstream applications. The mRNA was isolated using the NEBNext Poly(A) mRNA Magnetic Isolation Module (NEB, E7490) and then fragmented into RNA inserts of approximately 200 nucleotides. The cDNA libraries were constructed using the NEBNext Ultra RNA Library Prep Kit for Illumina (NEB, E7530) and NEBNext Multiplex Oligos for Illumina (NEB, E750). Sequencing was performed on the Illumina HiSeq sequencing platform. Reads were mapped to the rat genome using HISAT2 and StringTie software. Differential gene expression analysis was conducted using the DESeq2 package on the R platform. Enrichment analysis of differentially expressed genes (DEGs) in the transcriptome was performed using enrichR software.[33] The volcano plot, dot plot, and bar plot were generated using R software to visualize the results of the differential expression and enrichment analysis.

miRNA-mRNA Gene Prediction Network Analysis

We predicted the target genes of the top 20 most abundant ADEV miRNAs using four databases (miRWalk, miRTarbase, miRDB, and TargetScan). We then applied a pairwise intersection approach to identify predicted target genes. Specifically, we considered all possible pairwise combinations of the four databases, and, for each pair, we identified genes predicted by both databases and intersected them with DEGs from the bulk-seq dataset (using thresholds of log2FC ± 0.5 and P value < 0.05). The target genes identified in each pairwise intersection were then combined to form the final set of predicted target genes. Finally, Cytoscape software was used

Investigative Ophthalmology & Visual Science

Table 2. Primer Sequences Used for qPCR

Gene	Primer Sequences (F = Forward, R = Reverse)
PAK3	F: 5′-TTGGATAACGAAGAAAAACCCCC-3′
	R: 5′-GGGCACATCTGTGAGCCATAG-3′
THBS1	F: 5′-CAACGTGGTGAACGGTTC-3′
	R: 5′-TGTCCTGTAGCGTGGTCA-3′
Gstm1	F: 5′-ATACTGGGATACTGGAACGTCC-3′
	R: 5′-AGTCAGGGTTGTAACAGAGCAT-3′

to visualize the correlation network between ADEV miRNAs and retina mRNA datasets.

Quantitative PCR Analysis

Quantification of PAK3, THBS1, and Gstm1 was performed using total RNA extracted from retinal tissue lysates with the RNAiso Plus kit (Takara, Japan, 9108Q). For qPCR analysis, the SYBR Green Real-Time PCR Master Mix (Vazyme, Nanjing, China; Q712-032500) was used along with specific primers provided by Tsingke (Beijing, China). Gene expression was calculated using the formula $2^{-\Delta\Delta Ct}$. The primer sequences are listed in Table 2.

Statistical Analysis

The data are expressed as the mean ± standard error of the mean. Student's *t*-test for comparisons between two groups, and 1-way ANOVA with Tukey's post hoc test for comparisons involving three or more groups were carried out using GraphPad Prism (version 9.0.0, GraphPad Software, Boston, MA, USA, www.graphpad.com). Differences with $P < 0.05$ were considered statistically significant.

Results

Identification of Astrocytes and ADEVs

Immunocytochemistry confirmed that cultured astrocytes expressed GFAP and vimentin (Fig. 1A). NTA revealed that the ADEVs had a mean diameter of approximately 127.9 nm and a concentration of 2.8×10^{11} particles/mL (Fig. 1B). TEM revealed typical round and cup-shaped structures (Fig. 1C). Western blot (WB) analysis detected the EV markers Alix, TSG101, and CD81, whereas calnexin was absent (Fig. 1D), confirming the successful isolation of ADEVs.

ADEVs Protect Against GCC Thinning After Optic Nerve Injury

To investigate the neuroprotective role of ADEVs in RGC survival, we generated an ONC model and administered intravitreal injections of EVs at the time of injury (Fig. 2A). The image shows that we successfully conducted ONC, with the crush site indicated by a white arrow (Fig. 2B). PKH67-labeled ADEVs were distributed primarily in the ganglion cell layer (Fig. 2C). H&E staining revealed signif-

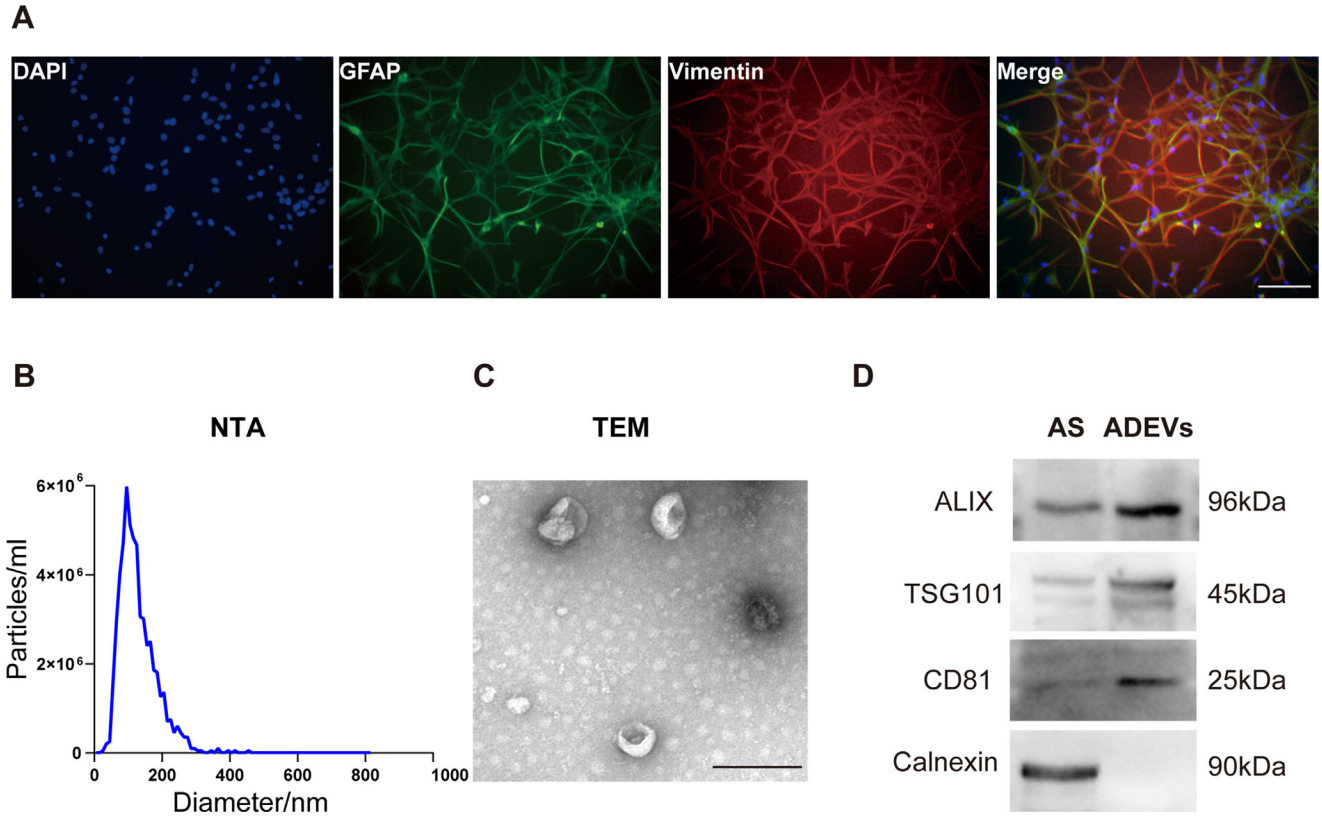

Figure 1. Isolation and characterization of extracellular vesicles from primary rat astrocytes. (**A**) Immunofluorescence was performed to identify primary astrocytes by double staining for GFAP (*green*) and vimentin (*red*); *blue* indicates the astrocyte nucleus. *Scale bar* = 100 µm. (**B**) Size distributions and particles of ADEVs as revealed by NTA analysis. (**C**) TEM was used to establish ADEV morphologies. *Scale bar* = 200 nm. (**D**) Western blotting was performed to detect the expression of Alix, TSG101, CD81, and calnexin in ADEVs and AS. ADEVs, astrocyte-derived extracellular vesicles; AS, astrocytes; GFAP, glial fibrillary acidic protein; NTA, nanoparticle tracking analysis; TEM, transmission electron microscopy.

Investigative Ophthalmology & Visual Science

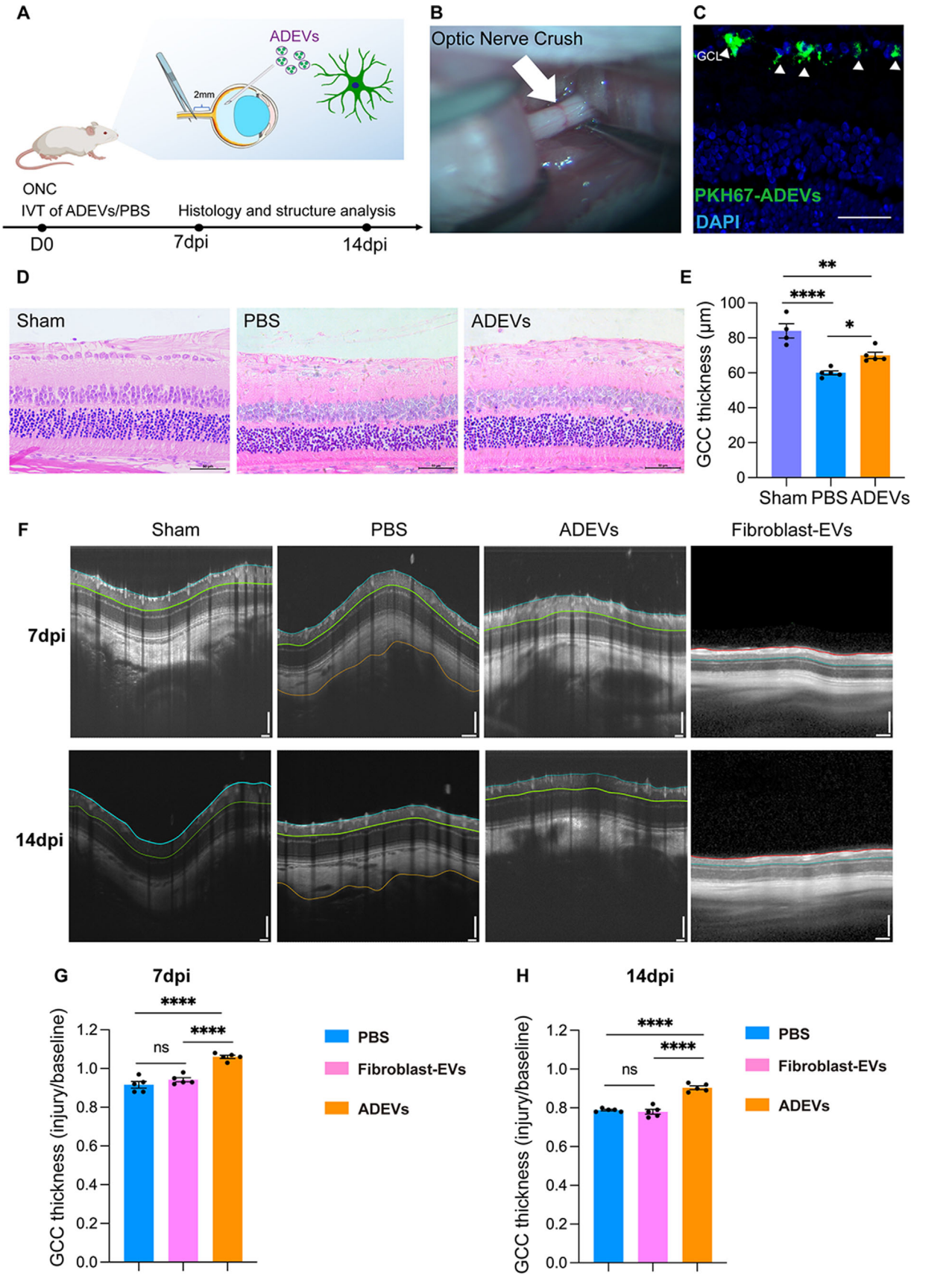

Figure 2. Protective effects of ADEVs on GCC thickness after optic nerve crush. (**A**) Schematic of animal experiments. (**B**) A representative image showing that the optic nerve was crushed; the injury site is indicated by a white arrow. (**C**) Distribution of PKH-67-labeled ADEVs in the retina. *Blue* indicates the nucleus, and *green* represents PKH-67-labeled ADEVs (*white triangle*). *Scale bar* = 50 μm. (**D**) H&E staining showing the central regions of retinal sections at 14 dpi in the sham/PBS/ADEV groups. *Scale bar* = 50 μm. (**E**) Statistical analyses

Investigative Ophthalmology & Visual Science

of the GCC thickness (H&E staining) of the central region at 14 dpi (sham: $n = 4$; PBS/ADEVs: $n = 5$). (**F**) GCC thickness was measured by OCT images, which revealed different retinal layers ranging from 1800 µm around the optic disc at 7 and 14 dpi. The extent of the reduction in GCC thickness on OCT was assessed by determining the ratio of 7 (**G**)/14 dpi (**H**) to baseline GCC thickness ($n = 5$/group). The data are presented as the means ± SEMs; $^{*}P < 0.05$, $^{**}P < 0.01$, $^{***}P < 0.001$, $^{****}P < 0.0001$ (one-way analysis of variance followed by Tukey's post hoc test). ADEVs, astrocyte-derived extracellular vesicles; dpi, days post injury; GCC, ganglion cell complex; GCL, ganglion cell layer; H&E, hematoxylin and eosin; OCT, optical coherence tomography.

icantly thicker GCC in the ADEV group than in the PBS group at 14 dpi in the central area (Figs. 2D, 2E). OCT assessments revealed a decrease in GCC thickness in the ADEV group compared with the PBS group at 7 dpi and 14 dpi, demonstrating the protective effect of ADEVs on RGCs (Figs. 2F, 2G, 2H).

ADEVs Protect Against the Progressive Loss of RGCs After Optic Nerve Injury

RGC survival was evaluated by counting RBPMS-positive cells in whole-mounted retinas. At 7 dpi, the ADEV group presented greater RGC densities in the peripheral region than did the PBS group, with no significant difference in the central and pericentral areas (Figs. 3A, 3B). At 14 dpi, significantly greater RGC densities were observed in the ADEV group across all retinal regions (see Figs. 3A, 3C). Retinal sections reconfirmed these findings (Figs. 3D, 3E), indicating that ADEVs mitigated progressive RGC loss after optic nerve injury.

To confirm the specificity of ADEVs, we compared RGC survival between PBS- and fibroblast-derived EV-treated rats after injury by measuring GCC thickness and counting RGC numbers in whole-mounted retinas. The results revealed no significant difference in GCC thickness or RBPMS-positive RGCs between the two groups (see Figs. 2F, 2G, 2H, 3A, 3B, 3C).

ADEVs Improved Visual Function in TON Rats

To assess the effect of ADEVs on visual function after injury, we recorded f-VEPs at 0 and 14 dpi (Fig. 3F). At 14 dpi, the ADEV group presented a significantly greater N1-P1 amplitude than the PBS group did, indicating that ADEV substantially preserved visual function following injury. No significant difference was observed between the groups on day 0 (Fig. 3G).

These findings highlight the efficacy of ADEVs in maintaining visual function after optic nerve injury.

Reactive Gliosis in the Retina

Glial cell activation is a key component of the neuroinflammatory response following optic neuropathies.[34] Immunofluorescence analysis revealed that, in the ADEV group, GFAP expression was elevated across all retinal layers at 7 dpi but remained high at 14 dpi (Figs. 4A, 4C, 4D). At 7 dpi, the ADEV group presented a significantly greater number of Iba1^{+} microglia than did the PBS group (Figs. 4B, 4E). Importantly, in both groups, microglia reactive to injury signals presented enlarged cell bodies and retracted processes. However, at 14 dpi, the number of Iba1^{+} microglia decreased in the ADEV group, and the microglia displayed a relatively homeostatic state (see Figs. 4B, 4F).

These results demonstrate that ADEV treatment can remodel retinal microenvironmental homeostasis by modulating glial cell responses after optic nerve injury.

RNA Sequencing Revealed Probable Neuroprotection-Related Mechanisms

To further explore the molecular mechanisms underlying the neuroprotective effects of ADEVs following optic nerve injury, we performed mRNA sequencing (mRNA-seq) to compare the retinal transcriptomes of the ADEV and PBS groups at 7 dpi. Using thresholds of $\log_2$-fold change ($\log_2$FC) > ±2 and P value < 0.05, we identified 81 upregulated genes and 53 downregulated genes in the ADEV group compared with the PBS group (Fig. 5A).

Gene Ontology (GO) enrichment analysis of the upregulated DEGs revealed significantly enriched biological processes, including positive regulation of macrophage chemotaxis, migration, granulocyte chemotaxis, and engulfment of apoptotic cells (Fig. 5B). Additionally, Kyoto Encyclopedia of Genes and Genomes (KEGG) pathway enrichment analysis revealed several pathways potentially related to neuronal injury or repair, such as the TGF-beta signaling pathway, necroptosis, axon guidance, the HIF-1 signaling pathway, and apoptosis (Fig. 5C).

Studies focused on the therapeutic effects of EVs in retinal diseases have highlighted their miRNA regulatory properties[25,35]; thus, we performed miRNA sequencing of ADEVs to investigate the role of miRNAs in ADEV-induced neuroprotection. Notably, the miRNA profile exhibited a highly concentrated expression pattern, with the top 20 miRNAs accounting for 85.3% of the total miRNA content (Fig. 5D).

Further functional enrichment analysis of the target genes of the top 200 miRNAs revealed biological processes associated with inflammation and neuroprotection, including positive regulation of cell migration and positive regulation of apoptotic processes (Supplementary Fig. S1A). KEGG pathway analysis also revealed pathways relevant to neuroinflammation and neuronal survival, such as the TNF signaling pathway, the PI3K-Akt signaling pathway, the NF-kappa B signaling pathway, the MAPK signaling pathway, and the neurotrophin signaling pathway (Supplementary Fig. S1B).

Furthermore, to explore potential targeting relationships between the highly expressed miRNAs and the differentially expressed mRNAs, we performed multidatabase predictive analysis on the top 20 highly expressed miRNAs (Supplementary Fig. S2A). We subsequently constructed a network diagram illustrating the interactions between the highly expressed miRNAs and the DEGs identified via mRNA-seq analysis (Fig. 5E).

Discussion

In this study, we investigated the neuroprotective role of ADEVs in an ONC model. Our findings show that ADEVs promote RGC survival and improve visual function. As

Investigative Ophthalmology & Visual Science

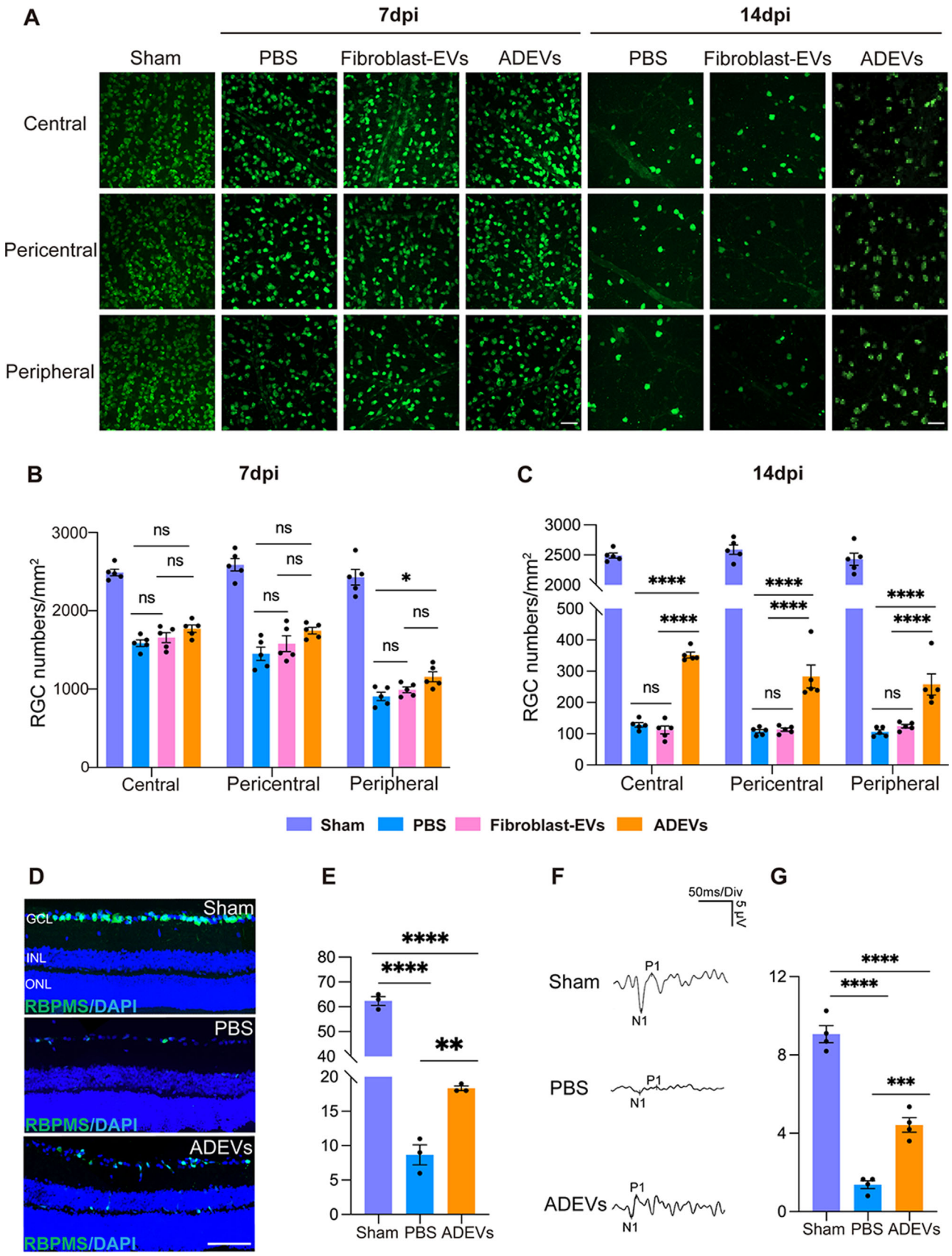

Figure 3. ADEVs prevented RGCs from progressive loss and improved visual function after ONC. (**A**) Immunofluorescence images showing RBPMS-labeled RGCs in retinal flat mounts in the sham/PBS/ADEV/Fibroblast-EV group at 7 and 14 dpi. *Scale bar* = 50 μm. (**B**) Statistical analysis of RBPMS-positive cells in 1 mm^2 areas (central/pericentral/peripheral) in retinal flat mounts at 7 dpi (n = 5/group). (**C**) Statistical analysis of RBPMS-positive cells in 1 mm^2 areas (central/pericentral/peripheral) of the whole retina at 14 dpi (n = 5/group).

(**D**) Representative images of RBPMS-positive cells in the GCL of the retina in the sham/PBS/ADEV groups at 14 dpi. *Scale bar* = 50 µm. (**E**) Statistical analyses of RBPMS-positive cell numbers in the 1 mm long GCL divided into the sham/PBS/ADEV groups (n = 3/group). (**F**) The f-VEP was used to record the N1-P1 amplitudes in the PBS and ADEV groups at baseline and 14 dpi. (**G**) Statistical analysis of N1-P1 amplitudes at baseline and at 14 dpi (n = 4). The data are presented as the means ± SEMs; *P < 0.05, **P < 0.01, ***P < 0.001, ****P < 0.0001 (one-way analysis of variance followed by Tukey's post hoc test). ADEVs, astrocyte-derived extracellular vesicles; dpi, days post injury; GCL, ganglion cell layer; INL, inner nuclear layer; ONC, optic nerve crush; ONL, outer nuclear layer; RGCs, retinal ganglion cells.

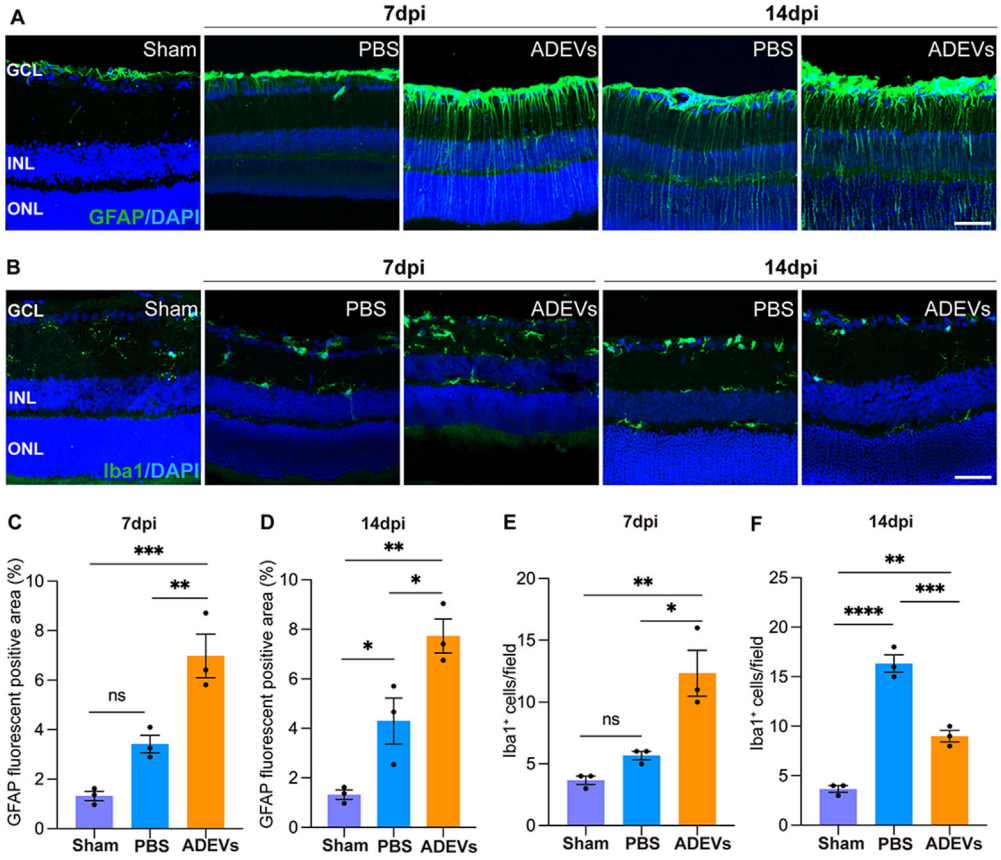

Figure 4. Reactive gliosis and inflammation of the retina after optic nerve crush and ADEV treatment. (**A**) Immunostaining showing the expression of GFAP (*green*) in the sham/PBS/ADEV groups at 7 dpi and 14 dpi. *Scale bar* = 50 µm. (**B**) Immunostaining showing the expression of Iba1 (*green*) in the sham/PBS/ADEV groups at 7 dpi and 14 dpi. *Scale bar* = 50 µm. Quantification of the GFAP fluorescent positive area (%) at 7 (**C**) and 14 (**D**) dpi (n = 3). Statistical analysis of Iba1+ cells at 7 (**E**) and 14 (**F**) dpi (n = 3). The data are presented as the means ± SEMs; *P < 0.05, **P < 0.01, ***P < 0.001, ****P < 0.0001 (one-way analysis of variance followed by Tukey's post hoc test). ADEV, astrocyte-derived extracellular vesicle; dpi, days post injury; GCL, ganglion cell layer; GFAP, glial fibrillary acidic protein; INL, inner nuclear layer; ONL, outer nuclear layer.

agents for cell-free therapy, ADEVs offer a promising new approach with greater specificity and lower oncogenic risk.

Influence of ADEV on Retinal Glial Cell Activation

After brain injury, astrocytes regulate microglial function through various mechanisms, influencing neuroinflammation and repair processes. Although microglia help attenuate neuroinflammation, over-activation can lead to the secretion of cytotoxic pro-inflammatory factors (e.g. ILs, TNF, NO, and ROS), exacerbating the injury. Astrocytes modulate microglial phenotypes by secreting cytokines and other molecules, promoting the shift from the neurotoxic M1 phenotype to the repair-oriented M2 phenotype, thus regulating the neuroinflammatory response.[36] Long et al. demonstrated that EVs from activated astrocytes promote microglial M2 phenotype transformation, expressing anti-inflammatory factors, such as Arg1, IL-4, and IL-10, which attenuate brain injury.[37] Additionally, microglia can induce the A1 reactive phenotype of astrocytes, further contributing to the cytotoxic environment.[38] Studies highlighted that EVs can mitigate the activation of neurotoxic A1 astrocytes, improving tissue preservation and recovery post-spinal cord injury.[39,40] Therefore, ADEVs have the potential to regulate the crosstalk between astrocytes and microglia, shifting them from a pro-inflammatory to an anti-inflammatory state. Retinal glial cells, including microglia, astrocytes and Müller cells, play critical roles in modulating the pathological process of TON,[4] exerting both neuroprotective and neurotoxic effects on RGCs. In our study, an ADEV treatment led to significantly increased GFAP expression at 7 and 14 dpi, indicating increased astrocyte and Müller cell activation. Reactive Müller cells express neurotrophic factors

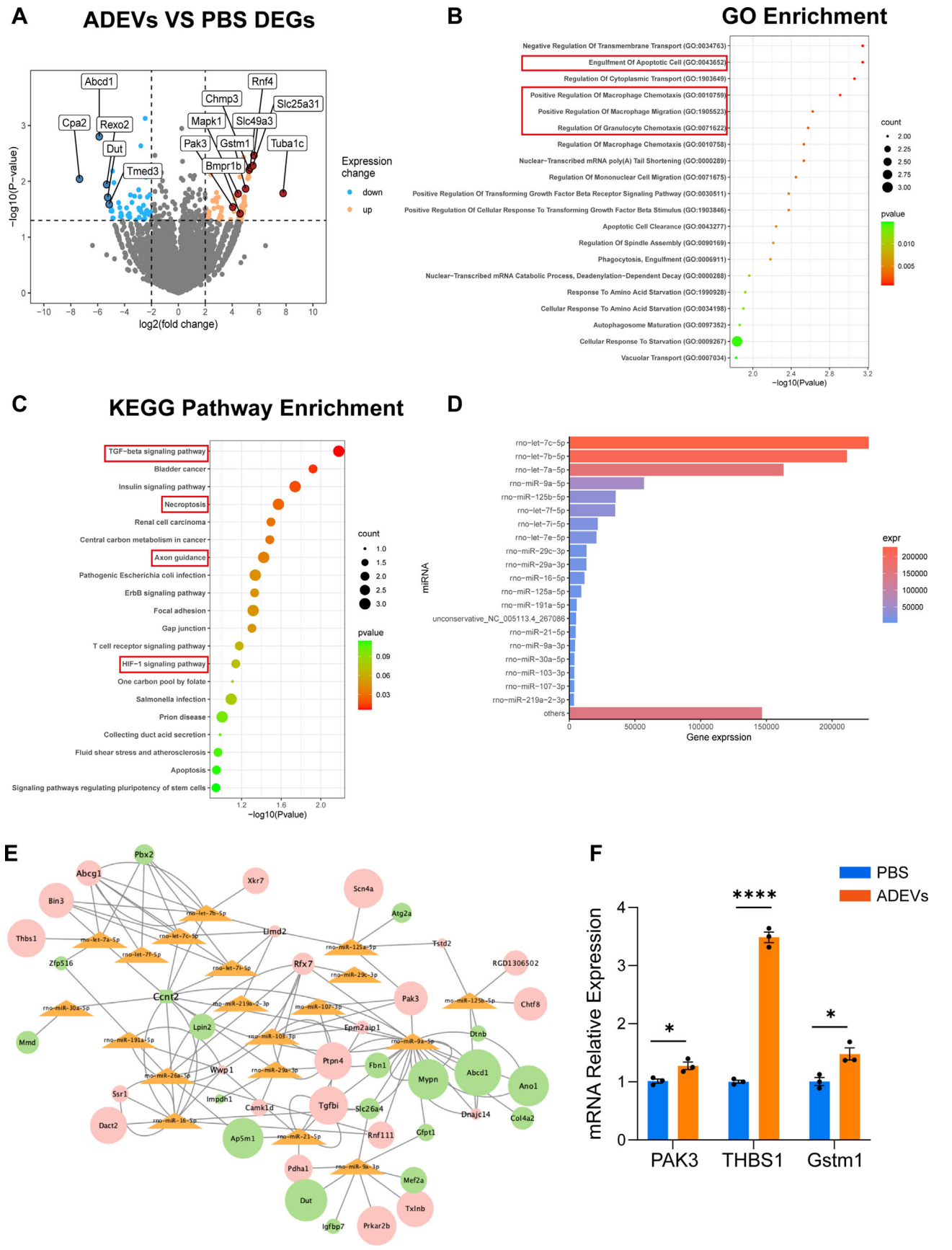

Figure 5. Transcriptomic and miRNA sequencing analyses revealed potential mechanisms of ADEV-mediated neuroprotection. (**A**)Volcano plot displaying DEGs identified by mRNA-seq of retinal tissue from the ADEV-treated and PBS-treated groups at 7 dpi. *Red* in the plots represents upregulated genes, and *blue* represents downregulated genes. (**B, C**) Dot plots illustrating GO biological process

terms and KEGG pathways enriched among the upregulated DEGs from the mRNA-seq analysis. The color of the dots reflects the significance of the enrichment, with *red* indicating lower *P* values (greater significance) and *green* indicating higher *P* values (less significant). (**D**) Bar plot showing the 20 most highly expressed miRNAs in the ADEV miRNA-seq data. (**E**) Network diagram illustrating the top 20 highly expressed miRNAs from the ADEV miRNA-seq data and DEGs from the mRNA-seq analysis. (**F**) The qRT-PCR assay results (PAK3, GSTM1, and THBS1). ADEV, astrocyte-derived extracellular vesicle; DEGs, differentially expressed genes; GO, Gene Ontology; KEGG, Kyoto Encyclopedia of Genes and Genomes.

in addition to BDNF, NGF, and GDNF, promoting RGC survival.[9,10] At the early stage of injury, astrogliosis can recruit microglia to injury sites and, at later stages, exert anti-inflammatory effects by modulating microglial activation. Recruitment of microglia promotes the tissue repair but can exacerbate neuronal damage as sustained microglial activation can result in excessive production of proinflammatory cytokines and ROS, exacerbating neuronal damage.[4,7] In our study, microglia numbers were greater at 7 dpi in the ADEV group but returned to a relatively homeostatic state by 14 dpi. We hypothesize that reactive astrocytes may recruit microglia to the damaged retina to facilitate debris clearance and tissue repair. As the injury response progresses, ADEVs may promote a shift in the astrocyte phenotype toward the neuroprotective A2 state, which in turn reduces microglial activation and mitigates prolonged inflammation. This dynamic interplay between astrocytes and microglia underscores the potential therapeutic benefits of ADEVs in regulating glial responses to support RGC survival following optic nerve injury.

mRNA and miRNA Profiles Revealed Potential Mechanism of ADEV Mediated RGC Protection

We identified potential key genes involved in the neuroprotective effects of ADEVs through bulk-seq differential gene expression and miRNA target gene prediction. These genes include PAK3, THBS1, and Gstm1. PAK3 is involved in synaptic development and remodeling, whereas THBS1 plays a crucial role in neuroprotection and axonal repair by regulating astrocyte reactivity and synapse formation after injury.[41,42] Gstm1, which is upregulated in ADEV-treated retinas, may contribute to increased retinal antioxidant capacity and protection against ROS-induced damage.[43–45] Notably, these protective genes are upregulated in the miRNA-mRNA targeting network, which appears counterintuitive, as miRNAs are generally believed to downregulate their target mRNAs. We hypothesize that the upregulation observed could reflect indirect miRNA-mRNA regulation rather than direct targeting, which warrants further investigation. The changes in the expression levels of these genes were consistent with the trend observed in mRNA sequencing (Fig. 5F), supporting the neuroprotective role of these genes in ADEV-treated retinas.

Our comparison of ADEV cargo with other EV studies that have shown a neuroprotective effect of EVs on RGCs after optic nerve injury revealed the common expression of let-7 family miRNAs and miR125b-5p, whereas miR-9a-5p was specifically expressed in ADEVs.[22,24] MiR-9a-5p may regulate the MAPK and PI3K-Akt pathways, which are essential for neuroprotection and inflammation regulation in CNS injuries.[46–49]

Despite these promising results, our study has several limitations. We utilized ADEVs derived from neonatal cortical astrocytes rather than adult retinal astrocytes. Future studies can use adult retinal astrocytes to better mimic the in vivo environment and to validate the translational potential of ADEV-based therapies for TON. Because the methods historically used to isolate retinal astrocytes are prone to interference with Müller cells, more effective isolation techniques are essential to obtain higher yields and purities of retinal astrocytes for research and therapeutic applications.[50,51] In addition, evaluations at 7 and 14 dpi may not fully capture the prolonged effects of ADEVs, as MSC-derived EVs have shown prolonged neuroprotective effects in parallel studies.[20,21,35,52,53] Considering that RGCs make up only 1% of the total retinal cell population, performing single-cell sequencing of RGCs to explain the potential protective mechanism is a more intuitive option.

In conclusion, our study demonstrated that ADEVs have significant neuroprotective effects on RGCs following optic nerve injury. Through comprehensive transcriptomic and miRNA profiling, we identified key signaling pathways that mediate the protective effects of ADEVs, highlighting their potential as agents for use in a cell-free therapeutic strategy for retinal neurodegenerative diseases.

Acknowledgments

The authors thank all the contributors and their families.

Supported by the National Key R&D Program of China (2021YFA1101200).

Disclosure: **L. Chen**, None; **Z. Yu**, None; **S. Zhu**, None; **S. Song**, None; **G. He**, None; **Z.-L. Chi**, None; **W. Wu**, None

References

1. Chen B, Zhang H, Zhai Q, Li H, Wang C, Wang Y. Traumatic optic neuropathy: a review of current studies. *Neurosurg Rev*. 2022;45(3):1895–1913.
2. Singman EL, Daphalapurkar N, White H, et al. Indirect traumatic optic neuropathy. *Mil Med Res*. 2016;3:2.
3. Van Gelder RN, Chiang MF, Dyer MA, et al. Regenerative and restorative medicine for eye disease. *Nat Med*. 2022;28(6):1149–1156.
4. Miao Y, Zhao G-L, Cheng S, Wang Z, Yang XL. Activation of retinal glial cells contributes to the degeneration of ganglion cells in experimental glaucoma. *Prog Retin Eye Res*. 2023;93:101169.
5. Guttenplan KA, Stafford BK, El-Danaf RN, et al. Neurotoxic reactive astrocytes drive neuronal death after retinal injury. *Cell Rep*. 2024;43(6):114299.
6. Chang J, Qian Z, Wang B, et al. Transplantation of A2 type astrocytes promotes neural repair and remyelination after spinal cord injury. *Cell Commun Signal*. 2023;21(1):37.
7. Ramirez AI, de Hoz R, Salobrar-Garcia E, et al. The role of microglia in retinal neurodegeneration: Alzheimer's disease, Parkinson, and glaucoma. *Front Aging Neurosci*. 2017;9:214.
8. Yazdankhah M, Shang P, Ghosh S, et al. Role of glia in optic nerve. *Prog Retin Eye Res*. 2021;81:100886.
9. Chun MH, Ju WK, Kim KY, et al. Upregulation of ciliary neurotrophic factor in reactive Müller cells in the

rat retina following optic nerve transection. *Brain Res*. 2000;868(2):358–362.
10. Bringmann A, Iandiev I, Pannicke T, et al. Cellular signaling and factors involved in Müller cell gliosis: neuroprotective and detrimental effects. *Prog Retin Eye Res*. 2009;28(6):423–451.
11. Vecino E, Rodriguez FD, Ruzafa N, Pereiro X, Sharma SC. Glia-neuron interactions in the mammalian retina. *Prog Retin Eye Res*. 2016;51:1–40.
12. Gómez RM, Sánchez MY, Portela-Lomba M, et al. Cell therapy for spinal cord injury with olfactory ensheathing glia cells (OECs). *Glia*. 2018;66(7):1267–1301.
13. Hastings N, Kuan W-L, Osborne A, Kotter MRN. Therapeutic potential of astrocyte transplantation. *Cell Transplant*. 2022;31:9636897221105499.
14. Alhadidi QM, Bahader GA, Arvola O, Kitchen P, Shah ZA, Salman MM. Astrocytes in functional recovery following central nervous system injuries. *J Physiol*. 2024;602(13):3069–3096.
15. Hering C, Shetty AK. Extracellular vesicles derived from neural stem cells, astrocytes, and microglia as therapeutics for easing TBI-induced brain dysfunction. *Stem Cells Transl Med*. 2023;12(3):140–153.
16. Wang X, Li A, Fan H, Li Y, Yang N, Tang Y. Astrocyte-derived extracellular vesicles for ischemic stroke: therapeutic potential and prospective. *Aging Dis*. 2024;15(3):1227–1254.
17. Kumar MA, Baba SK, Sadida HQ, et al. Extracellular vesicles as tools and targets in therapy for diseases. *Signal Transduct Target Ther*. 2024;9(1):27.
18. Kalluri R, LeBleu VS. The biology, function, and biomedical applications of exosomes. *Science*. 2020;367(6478):eaau6977.
19. Gratpain V, Mwema A, Labrak Y, Mucccioli GG, van Pesch V, des Rieux A. Extracellular vesicles for the treatment of central nervous system diseases. *Adv Drug Deliv Rev*. 2021;174:535–552.
20. Cui Y, Liu C, Huang L, Chen J, Xu N. Protective effects of intravitreal administration of mesenchymal stem cell-derived exosomes in an experimental model of optic nerve injury. *Exp Cell Res*. 2021;407(1):112792.
21. Yi W, Xue Y, Qing W, et al. Effective treatment of optic neuropathies by intraocular delivery of MSC-sEVs through augmenting the G-CSF-macrophage pathway. *Proc Natl Acad Sci USA*. 2024;121(6):e2305947121.
22. Li T, Xing H-M, Qian H-D, et al. Small extracellular vesicles derived from human induced pluripotent stem cell-differentiated neural progenitor cells mitigate retinal ganglion cell degeneration in a mouse model of optic nerve injury. *Neural Regen Res*. 2025;20(2):587–597.
23. Zhu S, Chen L, Wang M, et al. Schwann cell-derived extracellular vesicles as a potential therapy for retinal ganglion cell degeneration. *J Control Release*. 2023;363:641–656.
24. Mead B, Tomarev S. Extracellular vesicle therapy for retinal diseases. *Prog Retin Eye Res*. 2020;79:100849.
25. Mead B, Tomarev S. Bone marrow-derived mesenchymal stem cells-derived exosomes promote survival of retinal ganglion cells through miRNA-dependent mechanisms. *Stem Cells Transl Med*. 2017;6(4):1273–1285.
26. Chun C, Smith AST, Kim H, et al. Astrocyte-derived extracellular vesicles enhance the survival and electrophysiological function of human cortical neurons in vitro. *Biomaterials*. 2021;271:120700.
27. Chen W, Zheng P, Hong T, et al. Astrocytes-derived exosomes induce neuronal recovery after traumatic brain injury via delivering gap junction alpha 1-20 k. *J Tissue Eng Regen Med*. 2020;14(3):412–423.
28. Zhang W, Hong J, Zhang H, Zheng W, Yang Y. Astrocyte-derived exosomes protect hippocampal neurons after traumatic brain injury by suppressing mitochondrial oxidative stress and apoptosis. *Aging (Albany NY)*. 2021;13(17):21642–21658.
29. Lu Y, Chen C, Wang H, et al. Astrocyte-derived sEVs alleviate fibrosis and promote functional recovery after spinal cord injury in rats. *Int Immunopharmacol*. 2022;113(Pt A):109322.
30. Ramírez G, Toro R, Döbeli H, von Bernhardi R. Protection of rat primary hippocampal cultures from A beta cytotoxicity by pro-inflammatory molecules is mediated by astrocytes. *Neurobiol Dis*. 2005;19(1–2):243–254.
31. Baer ML, Henderson SC, Colello RJ. Elucidating the role of injury-induced electric fields (EFs) in regulating the astrocytic response to injury in the mammalian central nervous system. *PLoS One*. 2015;10(11):e0142740.
32. Welsh JA, Goberdhan DCI, O'Driscoll L, et al. Minimal information for studies of extracellular vesicles (MISEV2023): from basic to advanced approaches. *J Extracell Vesicles*. 2024;13(2):e12404.
33. Kuleshov MV, Jones MR, Rouillard AD, et al. Enrichr: a comprehensive gene set enrichment analysis web server 2016 update. *Nucleic Acids Res*. 2016;44(W1):W90–W97.
34. Shestopalov VI, Spurlock M, Gramlich OW, Kuehn MH. Immune responses in the glaucomatous retina: regulation and dynamics. *Cells*. 2021;10(8):1973.
35. Sang X, Tang L, Zhao L, et al. Umbilical cord mesenchymal stem cell-derived exosomes promote axon regeneration during optic nerve injury through microRNA-dependent mTORC1 signalling. *Clin Transl Med*. 2023;13(7):e1319.
36. Kumar A, Alvarez-Croda D-M, Stoica BA, Faden AI, Loane DJ. Microglial/macrophage polarization dynamics following traumatic brain injury. *J Neurotrauma*. 2016;33(19):1732–1750.
37. Long X, Yao X, Jiang Q, et al. Astrocyte-derived exosomes enriched with miR-873a-5p inhibit neuroinflammation via microglia phenotype modulation after traumatic brain injury. *J Neuroinflammation*. 2020;17(1):89.
38. Liddelow SA, Guttenplan KA, Clarke LE, et al. Neurotoxic reactive astrocytes are induced by activated microglia. *Nature*. 2017;541(7638):481–487.
39. Zhang J, Hu D, Li L, et al. M2 microglia-derived exosomes promote spinal cord injury recovery in mice by alleviating A1 astrocyte activation. *Mol Neurobiol*. 2024;61(9):7009–7025.
40. Yang Z, Liang Z, Rao J, et al. Hypoxic-preconditioned mesenchymal stem cell-derived small extracellular vesicles promote the recovery of spinal cord injury by affecting the phenotype of astrocytes through the miR-21/JAK2/STAT3 pathway. *CNS Neurosci Ther*. 2024;30(3):e14428.
41. Boda B, Alberi S, Nikonenko I, et al. The mental retardation protein PAK3 contributes to synapse formation and plasticity in hippocampus. *J Neurosci*. 2004;24(48):10816–10825.
42. Tyzack GE, Sitnikov S, Barson D, et al. Astrocyte response to motor neuron injury promotes structural synaptic plasticity via STAT3-regulated TSP-1 expression. *Nat Commun*. 2014;5:4294.
43. Buonfiglio F, Böhm EW, Pfeiffer N, Gericke A. Oxidative stress: a suitable therapeutic target for optic nerve diseases? *Antioxidants (Basel)*. 2023;12(7):1465.
44. Wu C, Han J, Wu S, et al. Reduced Zn2+ promotes retinal ganglion cells survival and optic nerve regeneration after injury through inhibiting autophagy mediated by ROS/Nrf2. *Free Radic Biol Med*. 2024;212:415–432.
45. Olson E, Pravenec M, Landa V, et al. Transgenic overexpression of glutathione S-transferase μ-type 1 reduces hypertension and oxidative stress in the stroke-prone spontaneously hypertensive rat. *J Hypertens*. 2019;37(5):985–996.

Investigative Ophthalmology & Visual Science

46. Fruman DA, Chiu H, Hopkins BD, Bagrodia S, Cantley LC, Abraham RT. The PI3K pathway in human disease. *Cell*. 2017;170(4):605–635.
47. Lee S-E, Lim C, Cho S. Angelica gigas root ameliorates ischaemic stroke-induced brain injury in mice by activating the PI3K/AKT/mTOR and MAPK pathways. *Pharm Biol*. 2021;59(1):662–671.
48. Xu S, Wang J, Zhong J, et al. CD73 alleviates GSDMD-mediated microglia pyroptosis in spinal cord injury through PI3K/AKT/Foxo1 signaling. *Clin Transl Med*. 2021;11(1):e269.
49. Qian Z, Chang J, Jiang F, et al. Excess administration of miR-340-5p ameliorates spinal cord injury-induced neuroinflammation and apoptosis by modulating the P38-MAPK signaling pathway. *Brain Behav Immun*. 2020;87:531–542.
50. Cullen PF, Mazumder AG, Sun D, Flanagan JG. Rapid isolation of intact retinal astrocytes: a novel approach. *Acta Neuropathol Commun*. 2023;11(1):154.
51. Foo LC, Allen NJ, Bushong EA, et al. Development of a method for the purification and culture of rodent astrocytes. *Neuron*. 2011;71(5):799–811.
52. Mead B, Ahmed Z, Tomarev S. Mesenchymal stem cell-derived small extracellular vesicles promote neuroprotection in a genetic DBA/2J mouse model of glaucoma. *Invest Ophthalmol Vis Sci*. 2018;59(13):5473–5480.
53. Wang T, Li Y, Guo M, et al. Exosome-mediated delivery of the neuroprotective peptide PACAP38 promotes retinal ganglion cell survival and axon regeneration in rats with traumatic optic neuropathy. *Front Cell Dev Biol*. 2021;9:659783.